

Influence of distortion on the electronic band structure of **CuInSe₂**.

H. Tototzintle-Huitle

Departamento de Física, CINVESTAV, México

J. Otálora

*Departamento de Física, Universidad Pedagógica
y Tecnológica de Colombia, Tunja, Colombia.*

J. A. Rodríguez

Departamento de Física, Universidad Nacional de Colombia, Bogotá, Colombia.

R. Baquero

rbaquero@fis.cinvestav.mx

(Date textdate; Received textdate; Revised textdate; Accepted textdate; Published textdate)

Abstract

We present a tight-binding calculation of the influence of distortion on the bulk electronic structure of the chalcopyrite CuInSe₂. We calculate the ideal case and then the effect of the inclusion of the distortions. We analyze our results in detail and conclude from a comparison with other work that the distortions must be included in the Hamiltonian to get a proper account of the electronic band structure. We use our new Hamiltonian to study the effect that both the tetragonal and the anionic distortion have on the (112) surface electronic band structure. We find this effect non-negligible..

I. INTRODUCTION

The quest for room temperature ferromagnetic semiconductors that can be matched to conventional semiconductors resulted in an increasing interest in $A^{II}B^{IV}C_2^V$ as well as in $A^IB^{III}C_2^{VI}$ chalcopyrites[1]. These materials are also interesting as non-linear optic devices, infrared photodetectors and in solar cell applications with a high efficiency-to-cost ratio[2, 3, 4, 5, 6, 7].

Chalcopyrites are tetragonal centered crystallographic structures with eight atoms in the unit cell basis. Their spatial group is the D_{2d}^{12} . The location and identification of the eight atoms in the CuInSe_2 unit cell is shown in Table IV below.

Chalcopyrites can deviate from their ideal symmetry in two ways. The c/a ratio can be different from its ideal value 2 and also the anion which lies in the middle of a tetrahedron can slide along the central axis. In this paper, we present a detailed study of a tight-binding calculation that includes the influence that both distortions have on the bulk electronic band structure of CuInSe_2 . It is straightforward to generalize this work to calculate their influence in the whole series of Cu-based chalcopyrites. The final result is a set of Hamiltonians precise enough for the whole series that allow to study different surfaces, monolayers and interfaces of these materials in more complicated systems and situations of current interest with a very simple method.

II. SOME DETAILS ON THE METHOD

We use the tight-binding method [8] to calculate the non-distorted as well as the distorted case. This method has been used before to describe chalcopyrites successfully [9, 10, 11, 12] as well as the related zincblende semiconductor compounds [13, 14]. $A^IB^{III}C_2^{VI}$

In the tight-binding method one constructs Bloch functions $\phi_v^\mu(\mathbf{k}, \mathbf{r})$ to describe an electronic orbital v centered at the position $\tau + \mathbf{d}_\mu$ of the ion labelled by μ , as a linear combination of atomic-like orbitals $\psi_v^\mu(\mathbf{r})$ [8]

$$\phi_v^\mu(\mathbf{k}, r) = \frac{1}{\sqrt{N}} \sum_{\tau} e^{i\mathbf{k} \cdot (\tau + \mathbf{d}_\mu)} \psi_v^\mu(\mathbf{r} - (\tau + \mathbf{d}_\mu)) \quad (1)$$

where \mathbf{k} is a Bloch vector in the First Brillouin Zone and N the number of unit cells in the crystal volume considered. We describe the group III metal In and the group IV anion with

atomic-like orbitals of s- and p³- symmetry. For Cu we consider a full s, p³, d⁵ basis. The spin-orbit interaction is responsible for a crystal field splitting of the heavy and light hole bands on the top of the valence band. It is not taken into account in our calculation since it is expected to be small. The matrix elements of the Hamiltonian have the form:

$$\int \phi_v^\mu(\mathbf{k}, \mathbf{r}) H \phi_{v'}^{\mu'}(\mathbf{k}', \mathbf{r}') d\mathbf{r} = \delta_{\mathbf{k}, \mathbf{k}'} \sum_{\mathbf{d}_{\mu, \mu'}} e^{i\mathbf{k} \cdot \mathbf{d}_{\mu, \mu'}} \langle \nu | \nu' \rangle_{\mathbf{d}_{\mu, \mu'}} \quad (2)$$

where

$$\langle \nu | \nu' \rangle_{\mathbf{d}_{\mu, \mu'}} = \int \psi_\nu^{\mu*}(\mathbf{r}) H \psi_{\nu'}^{\mu'}(\mathbf{r} - \mathbf{d}_{\mu\mu'}) d\mathbf{r} \equiv V_{\nu\nu'}^{\mu\mu'} \quad (3)$$

$\mathbf{d}_{\mu\mu'}$ is the position vector of the μ' atom from the μ atom. To calculate the non-diagonal matrix elements in 3 we use the Harrison's rule [15]. Therefore the interaction between an atomic-like orbital of symmetry x located at the site $\mu = 1$ (In) with another atom of symmetry y at $\mu' = 2$ (Se) is given by $V_{xy}^{12} = lm[V(pp\sigma) - V(pp\pi)]$. To actually calculate the tight-binding parameters, we use further $V(ij\alpha) = \eta(ij\alpha)\hbar^2/md_{\mu\mu'}^2$ ($d_{\mu\mu'}$ is the interatomic distance, m the electron bare mass) for s and p atomic-like orbitals. For the interaction between s, p with d orbitals, we use instead $V(id\alpha) = \eta(id\alpha)\hbar^2r_d^{3/2}/md_{\mu\mu'}^{7/2}$ (for r_d see Table III and ref. [15]). The $\eta(tw\alpha)$ parameters are given in [15]. If we go on and calculate the diagonal matrix elements using the same procedure, we get an inadmissible large value for the gap. If we try the tight-binding parameters proposed by Papaconstantopoulos [16] for Cu metal, we do not get the right gap as well. Also the Cu on-site parameters that reproduce correctly the electronic band structure of the superconducting perovskite. YBa₂Cu₃O₇ fail. Cu orbitals have an important influence on the gap edges in the electronic band structure of the Cu-based chalcopyrites.

In the semiconducting Cu-based chalcopyrites, the s-like orbital plays a mayor role in fixing the lower edge of the conduction band while the p-like one influences the position of upper edge of the valence band. The d-like Cu-orbital mostly fixes the value of the chalcopyrite gap. These orbitals and the p-like Se ones repel each other and push the upper valence band edge upwards so that the gap is diminished [17, 18, 19]. Consequently, we have

fixed the Cu on-site parameters for the whole series in such a way that we get the lowest possible deviation from the semiconducting gap. More exactly, we have selected the three Cu on-site parameters so that $\sum_{\text{series}} (E_{\text{series}} - E_{g_{\text{series}}}^E)^2$ as a function of E_{series} is minimum. $E_{g_{\text{series}}}^E$ are the experimental values of the gap. Small further adjustments of the anion (Se) p on-site parameter for each chalcopyrite allowed us to get the right experimental gap for the whole series. The experimental values that we used are quoted in the next Table I.

Chalcopyrite	$E_g^E [eV]$
<i>CuAlS₂</i>	3.49
<i>CuAlSe₂</i>	2.67
<i>CuAlTe₂</i>	2.06
<i>CuGaS₂</i>	2.43
<i>CuGaSe₂</i>	1.68
<i>CuGaTe₂</i>	1.23
<i>CuInS₂</i>	1.53
<i>CuInSe₂</i>	1.04
<i>CuInTe₂</i>	1.02

Table I- Experimental optical gap for the whole series of Cu-based chalcopyrites considered to set the tight-binding parameters [17].

The on-site tight-binding parameters that we get in this way are compared in Table II to the ones obtained from the Harrison's formulas [15].

Parameter	Harrison	This work
$E_s [eV]$	-6.92	-14.55
$E_p [eV]$	-1.83	-2.22
$E_d [eV]$	-20.14	-16.97
$r_d [\text{\AA}]$	0.67	1.15

Table II- The Cu on-site tight-binding parameters. The parameter r_d is defined in [15].

III. THE HAMILTONIAN

The Hamiltonian is labelled with the atom numbers in the following way. We take into account first nearest neighbors interactions only. The Hamiltonian matrix takes the form

	<i>In</i> 1	<i>Cu</i> 3	<i>Cu</i> 5	<i>In</i> 7	<i>Se</i> 2	<i>Se</i> 4	<i>Se</i> 6	<i>Se</i> 8
<i>In</i> 1	H_{11}	0	0	0	H_{12}	H_{14}	H_{16}	H_{18}
<i>Cu</i> 3	0	H_{33}	0	0	H_{23}^+	H_{34}	H_{36}	H_{38}
<i>Cu</i> 5	0	0	H_{55}	0	H_{25}^+	H_{45}^+	H_{56}	H_{58}
<i>In</i> 7	0	0	0	H_{77}	H_{27}^+	H_{47}^+	H_{67}^+	H_{78}
<i>Se</i> 2	H_{12}^+	H_{23}	H_{25}	H_{27}	H_{22}	0	0	0
<i>Se</i> 4	H_{14}^+	H_{34}^+	H_{45}	H_{47}	0	H_{44}	0	0
<i>Se</i> 6	H_{16}^+	H_{36}^+	H_{56}^+	H_{67}	0	0	H_{66}	0
<i>Se</i> 8	H_{18}^+	H_{38}^+	H_{58}^+	H_{78}^+	0	0	0	H_{88}

(4)

The diagonal sub-matrices are 9x9 for Cu and 4x4 for In and Se. The Hamiltonian matrix is altogether 42x42.

Obviously, $H_{33} = H_{55}$. These refer to Cu. $H_{11} = H_{77}$, they refer to In. $H_{22} = H_{44} = H_{66} = H_{88}$ which describe the Se atoms. The non-diagonal sub-matrices describe the first-nearest neighbors interactions. Their tight-binding parameters were computed from the Harrison's formulas [15]. The anion p-on-site parameter was adjusted further to get the exact experimental value (see below) With these data, the Hamiltonian can be built up straightforwardly [20, 21, 22].

IV. RESULTS

A. The ideal case

To get the experimental value for the gap (see Table II) in our calculated band structure we did a small (about 8%) further adjustment to the p-on-site parameter for the Se atom. The Harrison formula gives 9.53 eV to be compared with our 8.789 eV. The electronic band structure is presented in the next Fig. 1. There are 2 Cu, 2 In and 4 Se atoms in the unit cell. Each Se atom contributes with 2, each In with 3 and each Cu with 1s+5d occupied electronic states and therefore 26 bands in the valence band. The rest of the 42 bands (16) appear as empty conduction bands. The band structure appears in the next Fig. 1.

FIGURE 1

Both the top valence band and the bottom conduction band are approximately parabolic at Γ and therefore in some calculations the effective band approximation should be a good one. The semiconducting optical gap is direct and is calculated as the difference between the energies Γ_{1c} and $\Gamma_{4\nu}^{(2)}$ which is equal to 1.04 eV (a fitted value to the experimental one). The matrix element for dipolar transitions between these states, $\langle \Gamma_{4\nu}^{(2)} | \mathbf{r} | \Gamma_{1c} \rangle$ is different from zero along the z-axis (since z is an element of the Γ_4 representation; it is proportional to $\langle \Gamma_{4\nu}^{(2)} | \Gamma_4 | \Gamma_{1c} \rangle$ and $\Gamma_4 \otimes \Gamma_1 = \Gamma_4$) but equal to zero at Γ (since $\langle \Gamma_{4\nu}^{(2)} | z | \Gamma_{4\nu}^{(2)} \rangle \implies \langle \Gamma_4 | \Gamma_4 | \Gamma_4 \rangle$ and $\Gamma_4 \otimes \Gamma_4 = \Gamma_1$).

1. The valence band

Immediately below the singlet state $\Gamma_{4\nu}^{(2)}$ (at the top of the valence band), we find a doublet $\Gamma_{5\nu}^{(2)}$. The dipolar moment along z is different from zero ($\langle \Gamma_{5\nu}^{(2)} | z | \Gamma_{5\nu}^{(2)} \rangle \implies \langle \Gamma_5 | \Gamma_4 | \Gamma_5 \rangle$ and $\Gamma_4 \otimes \Gamma_5 = \Gamma_5$). Therefore the dipolar moment at the top of the valence band (a triplet in the zincblende parent compound) breaks into a zero dipolar moment at the top $\Gamma_{4\nu}^{(2)}$ and a non-zero one at the doublet $\Gamma_{5\nu}^{(2)}$. The operator representing the quadrupole moment is proportional to $3z^2 - r^2$ which belongs to Γ_1 and the products of the type $\langle \Gamma_x | \Gamma_1 | \Gamma_x \rangle$ are always different from zero since $\Gamma_1 \otimes \Gamma_x = \Gamma_x$ and so a non-zero quadrupole moment will exist for all the valence band states.

The 26 bands that conform the valence band are grouped together into three sub-bands separated by two in-band gaps. The first one (A in Fig.1) separates the upper valence band (UVB) from the middle valence band (MVB) and the in-band gap B separates this band from the lower valence band (LVB), At the top of the UVB there is a singlet, $\Gamma_{4\nu}^{(2)}$, separated from a doublet, $\Gamma_{5\nu}^{(2)}$, by a crystal field splitting, Δ_{cfs} , of 16 meV which is zero in the parent zincblende compound as we mentioned above. Notice that the doublet remains such from $\Gamma - Z$ but splits from $\Gamma - X$.

The chalcopyrite crystal field brakes the zincblende symmetry in several ways. First, there are two different cations instead of one which transforms the symmetry from cubic to tetragonal. Secondly, the anion can be found displaced along the center line of the tetrahedron that it forms together with the two different cations. But also the tetragonal symmetry ($\frac{c}{2a} = 1$ where c and a are the lattice parameters) is broken. We will deal with the effect of these distortions below.

a. The upper valence band (UVB) The splitting of the triplet in the zincblendes into the singlet $\Gamma_{4\nu}^{(2)}$ and the doublet $\Gamma_{5\nu}^{(2)}$ here, can be traced easily to be due to the presence a the two cations. This can be done with the tight-binding program replacing the parameters for Cu with those of In to get the bands for InSe or reversing the way we replace the parameters, we can get CuSe. In both cases the bands show a triplet on the top of the valence band at Γ . When the bands of the zincblende are compared to the ones of the chalcopyrite, we realize that two further splitting occur at the top of the valence band, one at Z (ΔZ in Fig. 1) and another one at X (ΔX).

There are 10 bands in the UVB that lie from 0 to -5 eV (the origin is set at the top of the valence band in Γ as it is customary). The main contribution comes from p-like Se orbitals. The details of the composition are in Fig.2 where the density of states (DOS) is shown. The shadow areas are proportional to the contribution of the orbital identified at the upper right corner.

b. The middle valence band (MVB) The inner-band gap A is small (16 meV, see Figs. 1 and 2). The MVB contains 12 bands; 10 of them are d-Cu orbital contributions. The deepest band of this group runs from $Z_{4\nu} + Z_{5\nu} \rightarrow \Gamma_{4\nu}^{(1)} \rightarrow X_{1\nu}^{(4)}$ as shown in Fig.1.

c. The lowest valence band (LVB) The deepest group of bands, the LVB, is separated from the MVB by a large gap from $\Gamma_{4\nu}^{(1)}$ to $\Gamma_{3\nu}$ of about 4eV. The main contribution comes from the s-Se orbitals (see Fig.2 for more details). The upper band of this group is a singlet $\Gamma_{3\nu}$ followed very closely by a doublet $\Gamma_{5\nu}^{(1)}$. In the zincblende parent compound these bands are degenerate. This splitting is due to the presence of a second cation. The upper band of this group $Z_{1\nu} + Z_{2\nu} \rightarrow \Gamma_{3\nu}$ is doubly degenerate from $Z - \Gamma$ but splits from $\Gamma - X$.

FIGURE 2

2. The conduction band

The conduction band (CB) minimum runs from $Z_{1c} + Z_{2c} \rightarrow \Gamma_{1c} \rightarrow X_{1c}^{(1)}$ which is a singlet all along $Z\Gamma X$. At Z , nevertheless the band is degenerate and splits to a higher-in-energy band that runs from $Z_{1c} + Z_{2c} \rightarrow \Gamma_{3c} \rightarrow X_{1c}^{(1)}$. At X the band is again degenerate but at Γ_{3c} it is a singlet. From Fig.2, we see that the CB is divided into two clearly defined sub-bands separated by an in-band gap of about 0.2 eV. Each sub-band presents two peaks. The DOS is quite higher in the upper part the spectrum. The lowest conduction band (LCB)

goes from roughly 1-5 eV. The upper conduction band (UCB) runs from about 5.2-12 eV. The lower peak of the LCB is composed mainly from s-Cu and s-Se orbitals in the 1-3.7 eV energy region and from s-In and s-Se in the higher energy region. In the low energy region of the UCB, the main contribution is from p-Cu orbitals and in the higher energy peak it is from p-In ones (see Fig.2 for more details).

3. Comparison with other work

Jaffe and Zunger (JZ) [17] made an *ab initio* calculation of the electronic band structure of the chalcopyrite CuInSe₂. Sometimes ab initio calculations do not get the semiconducting gap right. JZ got 0.98 eV. The experimental value is 1.04 eV. But otherwise, our calculation compares well with theirs. The valence band width ($\Gamma_{4\nu}^{(2)} - \Gamma_{\nu}^{(1)}$) is 14.8 eV in our work and 13.8 eV in theirs. Both calculations agree in the fact that the top of the VB which is a triplet in the zincblende parent crystal structure is split apart into a singlet at the top and a deeper doublet. The $\Delta_{cfs} = -0.08$ eV in JZ and -0.016 in this work. We will show below that the difference shrinks as an effect of the distortions (both anion and tetragonal which are considered by JZ). Yooder *et al.* [23] has calculated this crystal field splitting $\Delta_{cfs} = 0$ for the ideal case and $\Delta_{cfs} = +0.01$ eV when the tetragonal distortion ($\frac{c}{a} = 2.008$) is taken into account. In his case the bands are in a reverted order which means that the doublet is on the top of the valence band. This can be associated to his neglect of the anion distortion. There are some differences in both calculations. For example, for the width of the UVB we get 5 eV while JZ get 4 eV. This is actually the origin for the difference in the overall VB width. It is worth mentioning that the in-band gap A differs substantially in both works even qualitatively. The two bands that define this gap are reverted in JZ's work giving a -0.01 eV while we get a broad in-band gap of 1.67 eV. The overall width of the MVB does not differ very much. We get 1.5 eV and JZ 1.37 eV. On the other hand, the in-band gap B is higher in JZ (7.39 eV) while we get 4.79. Some of the differences are shown in detail in Table V below.

B. Influence of distortions

It is obvious that a correct description of the chalcopyrites must include the effect of distortions (both, the anion and the tetragonal one). In this section we will show the effect of this inclusion. The tetragonal distortion means that the ratio $\frac{c}{2a} = \eta \neq 1$ and the anion distortion means that the anion is not located exactly at $a(\frac{1}{2}, \frac{1}{2}, \frac{1}{4})$ and equivalent positions but rather at $a(u, \frac{1}{2}, \frac{\eta}{4})$. The new positions are shown in the next Table IV.

Nb.	atom	ideal	distorted
1	In	(0, 0, 0)	(0, 0, 0)
2	Se	$(\frac{1}{4}, \frac{1}{4}, \frac{1}{8})$	$(u, \frac{1}{4}, \frac{\eta}{4})a$
3	Cu	$(\frac{1}{2}, 0, \frac{1}{4})$	$(\frac{1}{2}, 0, \frac{\eta}{2})a$
4	Se	$(\frac{3}{4}, \frac{1}{4}, \frac{3}{8})$	$(\frac{3}{4}, \frac{1}{2} - u, \frac{3\eta}{4})a$
5	Cu	$(0, 0, \frac{1}{2})$	$(\frac{1}{2}, \frac{1}{2}, 0)a$
6	Se	$(\frac{1}{4}, \frac{1}{4}, \frac{5}{8})$	$(1 - u, \frac{3}{4}, \frac{\eta}{4})a$
7	In	$(\frac{1}{2}, 0, \frac{3}{4})$	$(0, \frac{1}{2}, \frac{\eta}{2})a$
8	Se	$(\frac{3}{4}, \frac{1}{4}, \frac{7}{8})$	$(\frac{1}{4}, \frac{1}{2} + u, \frac{3\eta}{4})a$

Table IV Positions of the atoms in the unit cell in the ideal and distorted case.

We use the same Hamiltonian described above with the same basis on each atom and introduce the changes that describe the corresponding distortions. We can use the same symmetry group to construct the Hamiltonian since X-ray experiments indicate that the space group is preserved [3, 4, 17, 24, 25, 26] in spite of the distortions present. In this case the Se-atom (the anion) will have its first nearest neighbors (the cations) at different distances. Namely,

$$R_{In \rightarrow Se} = R_{12} = a\sqrt{u^2 + \frac{(1 + \eta)^2}{16}} \quad (5)$$

$$R_{Se \rightarrow Cu} = R_{23} = a\sqrt{(u - \frac{1}{2})^2 + \frac{(1 + \eta)^2}{16}} \quad (6)$$

and the direction cosines that intervene in the calculation are given by:

Vector	l	m	n
R_{12}	$\frac{ua}{R_{12}}$	$\frac{a}{4R_{12}}$	$\frac{\eta a}{4R_{12}}$
R_{23}	$\frac{(\frac{1}{2}-u)}{R_{23}}$	$-\frac{a}{4R_{23}}$	$\frac{\eta a}{4R_{23}}$

Tabla IV The direction cosines once distortion is taken into account. These are equal always to $\frac{1}{\sqrt{3}}$ in the ideal case.

The phase factors are to be corrected accordingly. Now it is straightforward to construct the tight-binding Hamiltonian that includes both, the tetragonal as well as the anion distortion. We present in the next Fig.3 our results for the influence that the inclusion of distortion has on the electronic band structure of CuInSe₂.

FIGURE 3

The general picture of the bands is quite similar. The VB present the same three groups separated by two in-band gaps. We do not obtain an important reduction of the total band width (13.79 eV to be compare to the ideal case value of 13.8 eV). The conduction band is formed again by two groups separated by a small in-band gap. Also as a general trend, we can say that in several aspects the result including the distortions agrees better with the JZ calculation.

The first think to notice is that since the space group remains the same, the degeneracies at the high symmetry points Z , Γ , and X also remain as it is to be expected. On the other hand, we see that the distortions have a mayor or minor effect on almost all the bands. Distortion diminishes the optical gap and as a consequence we get 0.95 eV in closer agreement with the 0.98 eV of JZ . The experimental value to which we have fitted the on-site parameters in the ideal case is 1.04 eV. We could retouch the p-on site Se parameter to get the experimental gap value back. We present our results here without this further adjustment to leave sharp the picture of the effect of distortion.

In the UVB, the crystal field splitting $\Delta_{cfs} = -0.09eV$ (JZ got $-0.08eV$) in contrast to the ideal case value $-0.016eV$. So the distortions have a very important influence in this crystal field splitting. If we take into account the result by Yooder *et al.* [23] quoted above, then we can conclude that the most important factor that influences the crystal field splitting is the anion distortion. The ΔZ and ΔX splitting enhance due to distortions as can be seen from the enhancement of the top valence band details in Fig.3. This sub-band broadens and as a consequence the in-band gap A shrinks.

The next MVB appears to be still a very narrow band from the d-Cu orbitals mainly. The effect of distortions is here a minor one and it is related essentially to the slight shrinking of the total sub-band width which enhances but slightly the in-band gap B. Notice that the

band $Z_{4\nu} + Z_{5\nu} \longrightarrow \Gamma_{4\nu}^{(1)} \longrightarrow X_{1\nu}^{(4)}$ becomes almost flat as a result of the distortions.

In the LVB which contains 4 bands associated with s-Se orbitals the main effect is to invert the sign of the crystal field splitting which reverts the order between $\Gamma_{3\nu}$ and $\Gamma_{5\nu}^{(1)}$ so that now the doubly degenerate band is on top. We summarize the effect of distortion in Table VI where we compare the energy values for several bands that we get for the ideal case and for the result after distortions are included with the ones obtained by JZ.

State	JZ	Ideal	Distorted
UVB-maximum	(eV)	(eV)	(eV)
$\Gamma_{4\nu}^{(2)}$	0.00	0.00	0.00
$\Gamma_{5\nu}^{(2)}$	-0.08	-0.02	-0.09
$Z_{3\nu} + Z_{4\nu}$	-0.79	-1.93	-1.82
$X_{1\nu}^{(5)}$	-0.54	-1.83	-1.22
UVB-minimum			
$\Gamma_{4\nu}^{(1)}$	-5.15	-8.11	-7.89
$Z_{4\nu} + Z_{5\nu}$	-5.12	-7.98	-7.87
$X_{1\nu}^{(4)}$	-5.13	-7.92	-7.82
s-Se band			
$\Gamma_{2\nu}^{(1)}$	-13.03	-12.91	-12.82
$\Gamma_{3\nu}$	-13.06	-12.90	-12.90
$\Gamma_{1\nu}^{(1)}$	-13.83	-14.80	-14.79
$Z_{1\nu} + Z_{2\nu}$	-13.00	-12.91	-12.82
$Z_{5\nu}$	-13.46	-14.00	-13.99
$X_{1\nu}^{(2)}$	-13.20	-13.36	-13.38
$X_{1\nu}^{(1)}$	-13.31	-13.57	-13.47
Other values			
Width band s-Se at Γ	0.80	1.90	1.96
Gap A	-0.01	1.67	1.23
Gap B	7.39	4.79	4.94
Δz	0.5	0.11	0.27
Δx	0.4	0.26	0.37
$\Gamma_{5\nu}^{(1)} - \Gamma_{3\nu}$	0.03	-0.01	0.08

Table V Comparison between energy values at some high symmetry points in the ideal and distorted cases.

In the conduction band the major effect of distortion is to shrink the sub-band width of the s-Cu orbitals and to enhance the one corresponding to s-In orbitals. The in-band gap between the two enhances. We compare some CB values in the ideal case with the ones when the distortions are included in the calculation to show the effect of distortion and quote the corresponding values obtained by JZ in the next Table VI.

State	JZ	Ideal	Distorted
Conduction band	(eV)	(eV)	(eV)
$\Gamma_{1c} = E_g(gap)$	0.98	1.04	0.95
Γ_{3c}	3.24	3.77	3.25
$Z_{1c} + Z_{2c}$	2.76	3.14	2.83
$X_{1c}^{(1)}$	2.25	1.87	1.56

Table VI The effect of distortion in the Conduction Band.

C. The (112) surface

In the next Fig.4, we present our result for the effect that the distortions have on the electronic band structure of the (112) surface of CuInSe₂. The open circles are the ideal case and the black ones are the result when distortions are included. In general, distortions do affect the VB and the CB in a noticeable way.

FIGURE 4

Of great interests the effect of distortions on the surface states. The full line in Fig.4 represents the border of the bulk valence band (VB) and of the conduction band (CB). Three surface states denoted as 1SE, 2SE and 3SE in Fig.4 appear. The 1SE state starts at Γ somewhere in the middle of the semiconducting gap. Both 2SE and 3SE appear to be closer to the CB minimum. Somewhere in the interval K - J the 2SE state crosses the state 1SE and becomes the one nearest to the top of the VB. If we follow 1SE further on, we see an important influence of distortions on this state. Indeed, in the ideal case, 1SE enters the CB region and becomes a resonance while if distortions are included, the state remains within the energy gap region as a pure surface state. A similar effect occurs with the 3SE

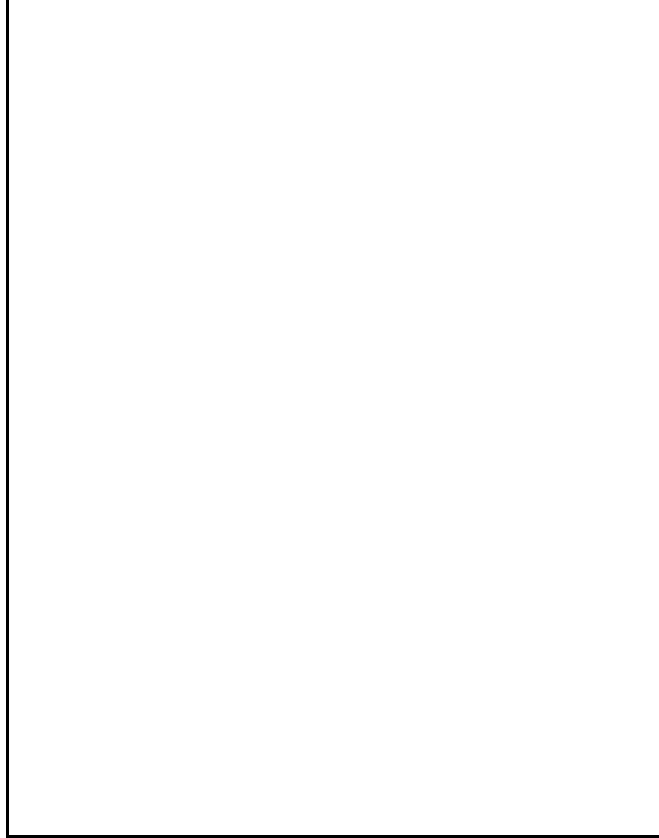


FIG. 1: Influence of distortions in the electronic band structure of the (112) surface of CuInSe_2 . Both, the tetragonal and the anion distortion are included. The open circles are the ideal result and the black ones the one with distortions included.

state around K which is a resonance in the ideal case but becomes a pure surface state as an influence of distortions. The 2SE state is switched towards the top of the VB when distortions are included. So the (112) CuTnSe_2 surface shows three pure surface states as a consequence of distortions that would partially become resonances would the lattice remain ideal. We conclude that distortions have an effect also in the surface states that is important and cannot be neglected.

V. CONCLUSIONS

We have studied the effect of distortion in the electronic band structure of the chalcopyrite CuInSe_2 . We find that its effect is important and that the inclusion of both the tetragonal and the ionic distortion are important to get a proper description of the electronic bands.

Once these are included we find that that the tight-binding Hamiltonian gives an accurate enough result to be useful for further calculations of surfaces, monolayers and interfaces and more complicated system that include this material. We have used the Hamiltonian together with the Green ´s Function Matching Method to calculate the effect of distortion on the (112) surface of this material. We find that distortions have an important effect on the three surface states that we found on this surface which is used in important technological applications.

-
- [1] Yu-Jun Zhao, and Alex Zunger, Phys. Rev. B **69**, 104422 (2004).
 - [2] W.H.Bloss, F. Pfisterer, and H. P. Hertlein, Photovoltaics: Solar Electricity, World Solar Summit ~Unesco, Paris, 1993.
 - [3] D. Haneman, CRC Crit. Rev. Solid State Mater. Sci. 14, 377,1988.
 - [4] A. Rockett and R. W. Birkmire, J. Appl. Phys. 70, R81-R97,1991.
 - [5] K. Zweibel, H. S. Ullal, and B. Von Roeden, 26th IEEE Photov.Spec.Conf.,Anaheim,CA.p.301,1997.
 - [6] J. Hedstrom, H. Ohlsen, M. Bodegard, A. Kylner, Lars Stolt, D.Hariskos, M. Ruckh, and W. Schock, in Proceedings of the 23rd IEEE Photovoltaic Specialist Conference, Louisville, KY(IEEE, Piscataway, NJ, 1993),p.364
 - [7] M. A. Contreras, A. M. Gabor, A. L. Tenant, S. Asher, J. Tuttle,and R. Noufi, Prog. Photovoltaics 2, 287(1994)
 - [8] C. Slater and G.F. Koster, Phys. Rev. **94**, 1498 (1954); F. Bassani and P. Parravicini, *Electronic States and Optical Transitions in Solids* (Oxford University Press, London, 1975).
 - [9] S. Froyen and W. A. Harrison, Phys. Rev. B **20**, 2420 (1979).
 - [10] F. A. P. Blom, H. Nachtgaele, and J.T. Devresse, Phys. Rev. B **32**. 2334 (1985).
 - [11] J.A.Rodriguez, L.Quiroga, A.Camacho y R.Baquero. Phys. Rev. B **59**,1555(1999)
 - [12] D.Olguin and R. Baquero, Eur.Phys.J.B **32**, 119 (2003)
 - [13] D.Olguin and R. Baquero, Phys. Rev. B **50**, 1980(1983).
 - [14] D.Olguin and R. Baquero, Phys. Rev. B **51**, 16891(1995).
 - [15] W.A. Harrison, *Electronic Structure and the Properties of Solids*. Dover Publications, Inc. New York, USA, 1989.

- [16] D. A. Papaconstantopoulos, *Handbook of the Band Structure of Elemental Solids*. Plenum Press, N. Y., 1986.
- [17] J. E. Jaffe and A. Zunger, Phys. Rev. B **28**, 5822 (1983).
- [18] J. E. Jaffe and A. Zunger, Phys. Rev. B **29**, 1882 (1984).
- [19] K. Yodee, J. C. Woolley, and Sa-Yakanit, Phys. Rev. B **30**, 5904 (1984).
- [20] J. A. Rodríguez, Rev. Mex. Fis. **45**, 584(1999).
- [21] J. A. Rodríguez, PhD. thesis, Universidad Nacional de Colombia, 1999 (unpublished).
- [22] Hugo Tototzintle-Huitile, PhD. thesis, Cinvestav, 2005 (unpublished).
- [23] K. Yodee, John C. Woolley, and Virulh Sa-Yakanit, Phys. Rev. B **30**, 5904(1984).
- [24] J. E. Jaffe and A. Zunger, Phys. Rev. B **29**, 1882(1984).
- [25] T. Ishi, Journal of Crys. Growth, **89**,459(1988).
- [26] T.F.Ciszek and C.D.Evans, Journal of Crys. Growth, **91**,533(1988).

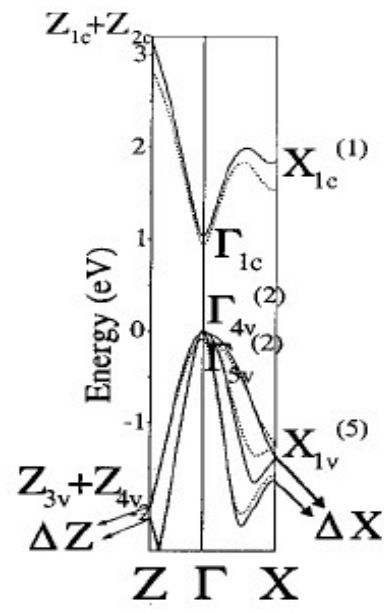
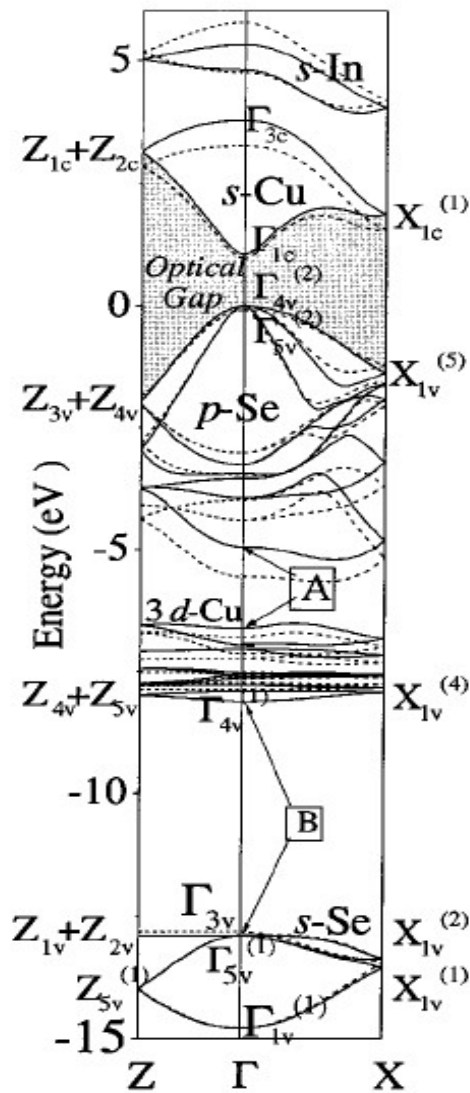
FIGURE CAPTIONS

Fig.1 The electronic band structure of CuInSe_2 .

Fig.2 Contribution to the DOS from the different orbitals at different energies.

Fig.3 Influence of distortion on the electronic band structure of CuInSe_2 . We used $u = 0.224$ and $\eta = 1.004$ (the ideal values are 0.25 and 1 respectively). The full line is the ideal case and the dot lines represent the effect of distortion.

Fig.4 Influence of distortions in the electronic band structure of the (112) surface of CuInSe_2 . Both, the tetragonal and the anion distortion are included. The open circles are the ideal result and the black ones the one with distortions included.



Energy(eV)

